High-Q whispering gallery mode germanium microresonators at 8 um

Dingding Ren[a,b], David Benirschke[a], Jae Ho Shin[a], and David Burghoff[a]

[a]Department of Electrical Engineering, University of Notre Dame, Notre Dame, Indiana, USA
[b]Department of Electronic Systems, Norwegian University of Science and Technology (NTNU), Trondheim, Norway

ABSTRACT

Achieving a high-quality (Q) factor for microresonators at a longer wavelength, e.g. longwave infrared (LWIR) with a wavelength from 8 to 14 um, will trigger new development in integrated non-linear optics and sensing on a chip. Although there are both powerful integrated light sources like solid-state quantum cascade lasers (QCLs) and strong driving force from chip-based sensing applications in the LWIR atmospheric transparent window,[1,2] the Q factors of the microresonators are only several thousand, due to limited choices of low-loss materials and complicated fabrication procedures.[3] Here, we report on the realization of a germanium (Ge) whispering gallery mode microresonator from a facile non-epitaxy fabrication process of high-quality Ge material with an ultra-smooth surface. By coupling the output of a QCL at 7.8 um into a partially suspended Ge on glass waveguide, an intrinsic Q of 2.5×10^5 are reported.[4] Compared with the previous study, our work shows the importance and great promise of maintaining high-quality material for integrated photonics at LWIR.

Keywords: Ge, microresonator, longwave infrared, non-epitaxy

1. INTRODUCTION

The long-wave infrared (LWIR) with wavelength spectrum from 8 to 14 um that is an ideal range of wavelength for both spectroscopic scientific research and industrial applications, as it covers the second atmospheric transparency window and the vibrational and rotational transition in molecules can be orders of magnitude stronger than near-infrared wavelengths. The fingerprints of molecules in LWIR include C_2H_4, TNT, and DNA , which are important for real-time environmental monitoring, explosive detection, and biomedical tests.[5,6] In contrast to the very successful and mature near-infrared (NIR) on-chip photonics, the compact and integrated LWIR optic and photonic devices are still in their infancy. Although there are integrable on-chip watt-level quantum cascade lasers (QCLs) available in LWIR at room temperature, the low fineness of the on-chip optical cavity requires quite an amount of input power that limits its wide chip-scale application in practical sensing[7] and supercontinuum generation.[8] In addition, frequency comb generated inside a ring or whispering gallery mode (WGM) microresonator in this spectrum could eliminate the frequency sweep with high coherence, sutiable for a variety of spectroscopic applications, like frequency comb ptychoscopy.[9–13] Compared with the Q factors of several millions using Si_3N_4 in NIR,[14] and Si operating up to 5 um,[15] both diamond and Ge have been made into whispering gallery mode microresonators and micro-ring resonators in LWIR. However, only several thousands of Q factors in LWIR were reported, which are far from the theoretical absorption limit of the intrinsic materials.[16–18]

Ge is a promising material platform with the highest refractive index of 4 and giant non-linear coefficients.[19] In addition, it has a wide low-loss transparency window from 2 to 14 um, covering the whole spectrum of LWIR.[3] To fabricate Ge-based on-chip photonic devices, heterogeneous integration is essential to make micro-structures for the confinement of light. Recently, epitaxy-grown Ge on GaAs and Si has been popular for making integrated waveguides and ring resonators. The optical mode was confined mostly in the low-loss Ge part, achieving waveguide loss around 4 dB/cm in LWIR.[20–22] However, these values may still be orders of magnitude larger than that from the highly resistive Ge grown by the traditional Czochralski crystal pulling method under

Send correspondence to D. Ren with e-mail: dren@nd.edu

thermodynamic equilibrium conditions. Although the epitaxial Ge layer is atomically smooth, either GaAs or Si was used as the substrate for heteroepitaxy, causing inevitable degradation for LWIR transparency. For Ge grown on GaAs, the volatile arsenic background, and the Ga interdiffusion causes unwanted impurity incorporation, lowing the optical transparency at LWIR.[23] Although Ge grown on Si will not be impacted by the unwanted background impurity incorporation like on GaAs, there is a significant lattice mismatch between Si and Ge, resulting in high-density of threading dislocation and lowering the material quality significantly.[24] To benchmark the absorption loss of Ge in LWIR, it is necessary to exploit the performance of Ge microcavity using high-quality and low-loss material and minimize any damage during the fabrication processes.

Here, we report on a successful fabrication of a Ge WGM microresonator integrated on glass. We maximize the utilization of nanomechanical fabrication processes of wafer bonding, lapping, and polishing. The fabricated microresonators show ultra-smooth surfaces, and they were lifted from the glass substrate surface by using hydrofluoric acid (HF) etching. To evaluate the optical properties of the resonator, we performed the transmission measurement by focusing the laser emission at around 7.8 um from a QCL into a partially suspended Ge waveguide, which was placed close to the resonator for efficient coupling of laser light into the microresonator. By sweeping the wavelength of the QCL, a loaded Q of 2.2×10^5 and an intrinsic Q of 2.5×10^5 were measured.

2. DEVICE FABRICATION

To make Ge WGM microresonators using the wafer bonding technique, both a good etching selectivity and similar thermal expansion coefficients between the bonding substrate and Ge are preferred. We chose SD-2 glass from Hoya Candeo Optronics Corporation as the bonding substrate, because its thermal expansion coefficient has been matched to Ge and there is a good etching selectivity between Ge and glass using hydrofluoric acid.[24] Figure 1 shows the schematic of the fabrication process. A piece of SD-2 glass of 1.5×1.5 cm^2 in size and 1 mm in thickness was firstly cleaned by acetone and IPA and a hot bath in H_2O_2:NH_4OH:H_2O solution with volume ratio of 1:1:5 at 90 C° for 15 min was followed. This step is to make sure that the surface of the glass is of high surface energy, favorable for hydrophilic bonding.[25] Then, a piece of highly resistive Ge around 1×1 cm^2 in size and 500 µm in thickness (purchased from Umicore using Czochralski method) was dipped into the same H_2O_2:NH_4OH:H_2O solution at room temperature for 5 seconds. We emphasize here that the surface treatment of Ge at a higher temperature or longer time will lead to surface degradation. After the surface treatment, the glass and Ge piece were sandwiched into graphite plates inside a homemade bonder. Then, 3000 N force was applied. The bonder was heated to 300 C° for 60 min.

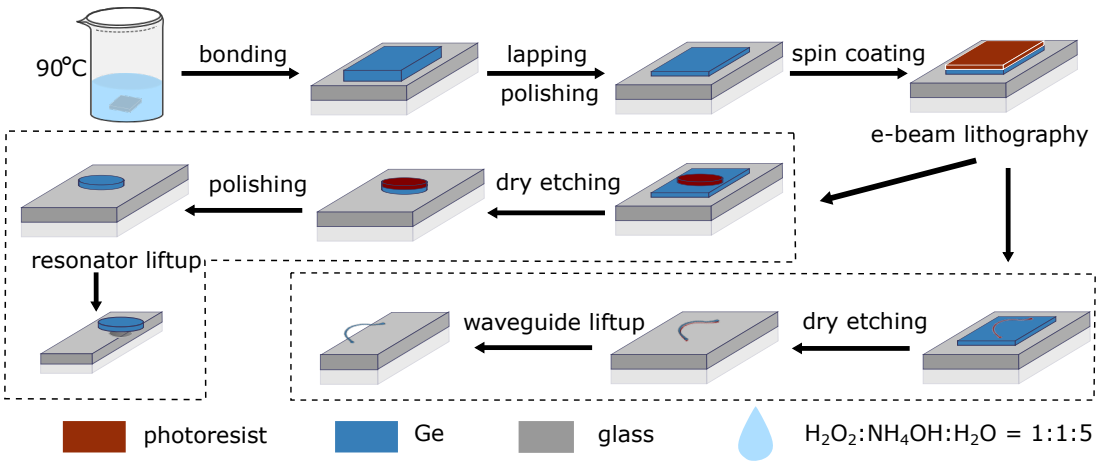

Figure 1. Overview of the fabrication procedure, which relies on a combination of wafer bonding and polishing. Reprinted from Ref. 4

Electron beam lithography was used to define the feature of the Ge microresonator on a Vistec EBPG5200 Electron Beam Lithography System at 100 KV. HMDS adhesion promoter and Espace-300Z discharger are essential to be applied before and after the spin-coating process of the e-beam resist ma-N 2403. An SF_6 chemistry

in the DRIE system has been used to etch through the Ge layer to define the feature of the microresonator. To ensure all the facets of the resonator have been finished with a polished smooth surface, the etched microresonator was loaded back to the lapping station for a final polishing step for 3 min. Then, the sample was put through an iteration of 3 times of HF etching and sidewall passivation process to etch back the glass layer and lift the edge of the resonator away from the glass. 49% HF was used for 1 min in each etching step and a flood exposure with positive S1813 photoresist has been used to passivate the vertical sidewall using a microresonator as a mask. This iteration of etching and passivation prevents severe in-plane etching that could easily wash away the resonator and keeps effective etching speed in the vertical direction.

Since Ge has the highest refractive index of 4, it will be extremely challenging to couple the light from other materials of lower refractive index into the Ge microresonator due to the requirement of the phase-matching condition.[19] In this regard, we fabricated a curved Ge waveguide using the same fabrication process described above to couple the light from the free space into the microresonator. The Ge waveguide has a larger in-plane end facet to enhance the collection of the light from the free space. To facilitate the approaching of the microresonator to the waveguide, both coupling sections of the Ge microresonator and waveguide have been diced to the edge of the glass chips. Then, an HF etching process has been used to further lift the Ge microresonator and to make the coupling area of the Ge waveguide suspended out from the glass chip. The suspended structure not only makes the coupling easier, but also provides bending tolerance of the waveguide that prevents rigid crashing with Ge microresonators.

3. MORPHOLOGICAL CHARACTERIZATION AND MODE SIMULATION

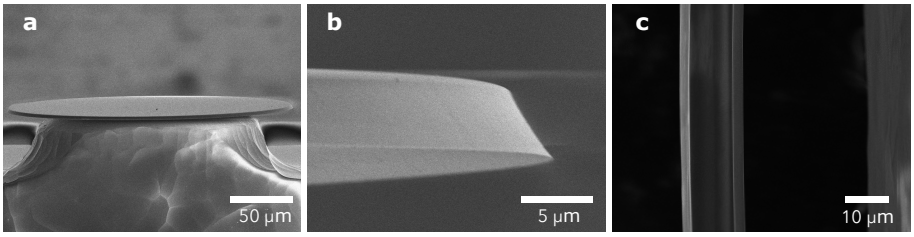

Figure 2. **a.**SEM image of a non-epitaxial Ge microresonator. The 450 µm disk is supported by a glass pillar. **b.**Magnified view of the microresonator edge where the WGM mode resides. **c.**Top view of the suspended Ge waveguide. The waveguide is on the left and the glass substrate is on the right. Reprinted from Ref. 4

The scanning electron microscopy (SEM) image of the slightly forward-tilted side view of a fabricated Ge WGM microresonator with a diameter of 450 µm can be seen in Fig.2**a**. The resonator has a uniform thickness across the whole resonator with the edge part in suspension. The suspended part is around 100 um away from the dune-shaped glass supporting structure in the center, excluding the interference with any lossy materials at LWIR. To look at the active part of the WGM microresonator, we slightly tilted the microresonator backward and zoomed in to the edge of the WGM microresonator. The SEM image in Fig.2**b** shows that the edge facet is about a 30-degree incline inward. This tilted side facet should result from a combination of the isotropic effect from dry etching and edge rounding effect from the polishing process. By changing the plasma etching anisotropic strength and polishing pressure, the geometry could be further tuned with the potential for dispersion engineering. Since the bottom side of the WGM microresonator has only gone through the wafer bonding process and it should be as close as the as-received polished surface condition of the Ge wafer, we did not find a significant surface roughness difference between the side-facet and the bottom facet in SEM, indicating potentially low scattering losses. To efficiently couple the light in LWIR to the WGM microresonator, we fabricated a partially suspended Ge waveguide on a glass chip with a dimension of 4×2 cm^2. The waveguide is around 5 um thick and 10 um wide, similar to that of the WGM microresonator. A higher magnification SEM image of the suspended part of the waveguide is shown in Fig. 2**c**, presenting uniform geometry and smooth surface, the beneficiary for coupling experiments.

Based on the geometry and dimension shown in Fig.2, we use the finite element method (FEM) and COMSOL Multiphysics software to simulate the light propagation in both the WGM microresonator and the Ge waveguide.

Since the electric field of the laser from our QCL is polarizing perpendicular to the propagation direction, we will only simulate the TE mode for both the WGM microresonator and the waveguide in this study. Figures 3**a** and **b** show the simulated mode profile of the WGM inside the microresonator and guided-mode inside the waveguide, respectively. The effective refractive index calculated based on the eigenfrequencies is about 3.88, which is close to the effective mode index of 3.92 in the waveguide, suggesting that the phase match condition has been met well.

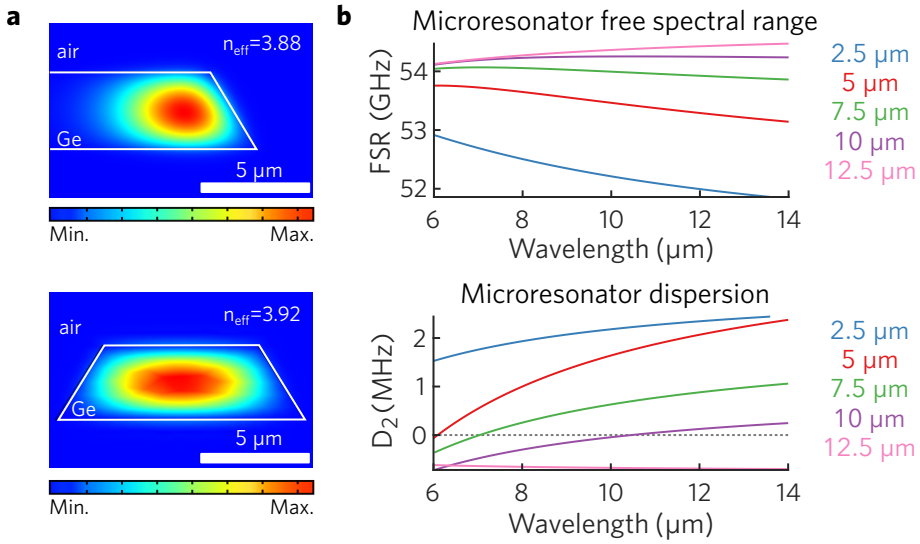

Figure 3. **a.** FEM simulation of the guided mode in the Ge. WGM microresonator and Ge waveguide. **b.** Calculated free spectral range and dispersion versus waveguide thickness. Low anomalous dispersion is only possible with very thick waveguides. Reprinted from Ref. 4

4. OPTICAL TRANSMISSION MEASUREMENTS

A single-mode distributed feedback QCL laser with emission wavelength from 1285.5 to 1290.5 cm^{-1} has been used to characterize the WGM microresonator. The schematic of the optical measurement setup is shown in Fig. 4**a**. Emitted collimated laser beam was expanded through two off-axis parabolic (OAP) mirror pairs by 10 and 2 times, consecutively, reaching a beam size of about 30 mm. Then, the collimated beam was focused to the entrance facet of the fabricated Ge waveguide using 1 inch OAP mirror with a focused beam size of about 300 μm^2. The transmitted laser signal from the waveguide was collected by an OAP of 4-inch focal length, and then the collimated beam size was reduced by 2 times using a pair of OAPs with 4-inch and 2-inch focal length in a series. Then, the transmitted signal was focused onto the Mercury-Cadmium-Telluride (MCT) detector, which was connected to a lock-in amplifier system to increase the signal-to-noise ratio. We further used two tunable pinholes at the confocal planes of two OAP mirror pairs to exclude the unwanted interference from the scattered laser signal in the system. The photograph in Fig. 4**b** shows the side view of the experimental setup for the coupling experiment. The 1-inch objective OAP mirror is on the right side, the waveguide is mounted on the metal post in the front, and the WGM microresonator is mounted on the yellow piezo actuator at the back. The 40 × objective lens has been mounted on the top of the waveguide to monitor the relative in-plane position between the resonator and waveguide. Since the side facet of the WGM microresonator is about 30 ° tilted, it will be beneficiary for coupling if the waveguide is placed below the WGM microresonator. Figure 4**c** shows the optical image when the WGM microresonator is placed on top of the waveguide. By changing the piezo voltage, we can tune the position of the relative position of WGM microresonator to control the coupling strength. The transmission experiments have been performed using both TE and TM polarizations by tuning the mounting angle of the QCL. Figure 4**a** and **b** show the normalized transmission signal from the waveguide-WGM microresonator system. The lasing wavelength was tuned by changing the temperature and the current of the QCL. A pair of major transmission dips can be found at the wavelength of 1285.4 cm^{-1} and

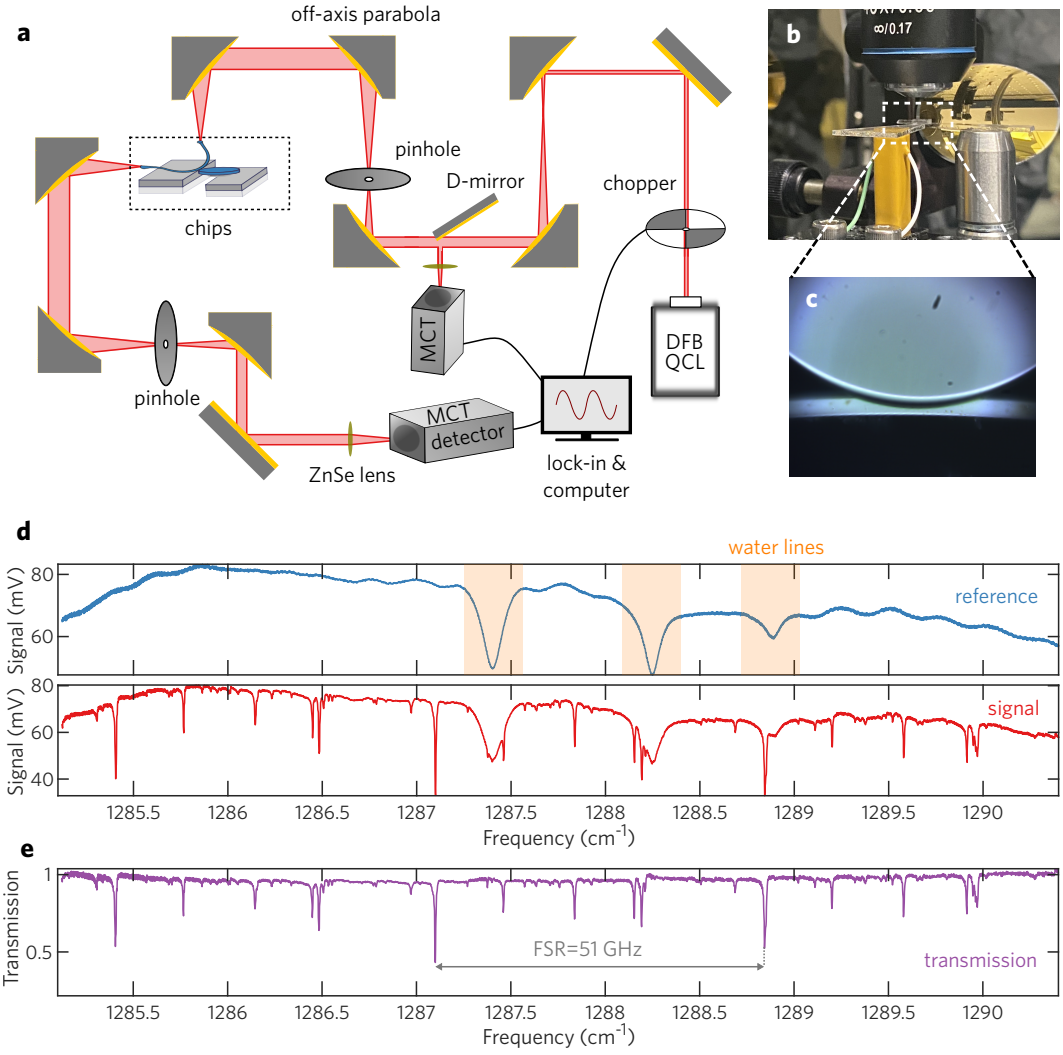

Figure 4. **a**. Schematic of the optical path and components. A DFB QCLis focused into the waveguide and coupled to the resonator. **b**. Photograph of the coupling setup. **c**. Optical image of the Ge WGM microresoantor and waveguide when coupled, taken from the objective above the coupling area shown in **b**. **d**. Two consecutive wavelength-tuning scans when the microresonators was away (reference) and approached (signal) to the waveguide. **e**. Normalized transmission scan from **d**. Reprinted from Ref. 4

1287.1 cm^{-1} with a frequency separation of 51 GHz, which matches well to the 53 GHz free spectral range (FSR) of the WGM microresonator with a diameter of 450 µm, confirming that the transmission features are from the coupling between the waveguide and WGM microresonator. The loaded Q factors of the TE and TM mode of the WGM microresonator are estimated to be 221,130 and 224,170 by fitting the main transmission dips using the Lorentzian function in Fig. 5**a** and **b**, respectively. To figure out the coupling condition, we performed a series of transmission measurements by changing the piezo stage's voltage, which in turn changes the separation between the WGM microresonator and the waveguide. Figure 4**c** shows the transmission versus relative waveguide distance, and we can see a monotonic increase of the transmission over the range we can measure. This suggests that the 60% transmission is in an under-coupled condition. That transmission dips corresponding to higher-order modes with FSR smaller than 51 GHz start to grow significantly near the critical coupling point, suggesting severe parasitic coupling between the waveguide mode and the higher-order WGM modes. We used the transmission of 60% transmission spectra in Fig. 5**a** and **b** to calculate the intrinsic Q

factor with the equation

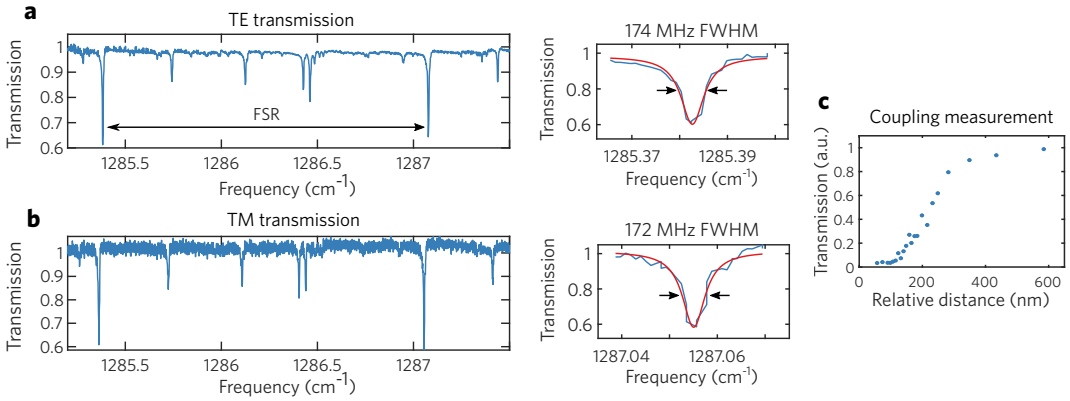

Figure 5. **a.** TE polarizationtransmission,with a FWHM linewidth of 174MHz. **b.** TM polarization transmission, with a FWHM linewidth of 172 MHz. **c.** Trend of transmission versus the change of vertical distance between the microresonator and waveguide. Due to the very high index mismatch between germanium and air,critical coupling is achieved only with in a very short distance. Reprinted from Ref. 4

$$Q_i = \frac{2Q_l}{1+\sqrt{T}}, \tag{1}$$

where Q_l is the loaded Q factor, and T is the normalized transmission in the under-coupled conditions. Based on the values acquired, the WGM microresonator shows intrinsic Q factors of 250610 and 252910 for TE and TM modes, respectively. These values are almost two orders of magnitude higher than those from previous microresonators in LWIR, which are summarized in table 1. The Q value of 2.5×10^5 corresponds to a total loss of 0.5 dB/cm, which is much lower than the Ge waveguide losses on both Si and GaAs.

5. SUMMARY

In short, we present a facile non-epitaxial fabrication process of Ge WGM microresonator and partially suspended waveguide. The Ge WGM microresonator has a uniform thickness with an ultrasmooth polished surface. By performing the transmission measurement of a waveguide, which is coupled to the WGM microresonator, we have observed transmission dips with repetition rate matched well to the FSR of WGM microresonator. Loaded Q factors of 221,130 and 224,170 have been measured for TE and TM modes, respectively, corresponding to the intrinsic Q factors of 250,610 and 252,910. These excellent Q values represent a milestone for high-quality LWIR optical cavities, which are important for integrated sensing and non-linear photonics on-chip.

ACKNOWLEDGMENTS

This work is sponsored by the Research Council of Norway through the FRIPRO Program (Grant No. 302923). D.R. thanks the generous financial support from the FRIPRO Mobility Fellowship, Research Council of Norway. D.B. acknowledges support from AFOSR grant no. FA9550-20-1-0192, NSF grant ECCS-2046772, and ONR grant N00014-21-1-2735.

REFERENCES

[1] Yao, Y., Hoffman, A. J., and Gmachl, C. F., "Mid-infrared quantum cascade lasers," *Nature Photonics* **6**(7), 432–439 (2012).

[2] Kaplan, H., [*Practical applications of infrared thermal sensing and imaging equipment*], vol. 75, SPIE press (2007).

[3] Soref, R., "Mid-infrared photonics in silicon and germanium," *Nature photonics* **4**(8), 495–497 (2010).

[4] Ren, D., Dong, C., and Burghoff, D., "High-q longwave infrared microresonators based on a non-epitaxial germanium platform," *arXiv preprint arXiv:2111.00362* (2021).

[5] Brown, S. S., "Absorption spectroscopy in high-finesse cavities for atmospheric studies," *Chemical reviews* **103**(12), 5219–5238 (2003).

[6] Brogna, R., Oldenhof, H., Sieme, H., and Wolkers, W. F., "Spectral fingerprinting to evaluate effects of storage conditions on biomolecular structure of filter-dried saliva samples and recovered dna," *Scientific reports* **10**(1), 1–12 (2020).

[7] López-Lorente, Á. I. and Mizaikoff, B., "Mid-infrared spectroscopy for protein analysis: potential and challenges," *Analytical and bioanalytical chemistry* **408**(11), 2875–2889 (2016).

[8] Della Torre, A., Sinobad, M., Armand, R., Luther-Davies, B., Ma, P., Madden, S., Mitchell, A., Moss, D. J., Hartmann, J.-M., Reboud, V., et al., "Mid-infrared supercontinuum generation in a low-loss germanium-on-silicon waveguide," *APL Photonics* **6**(1), 016102 (2021).

[9] Burghoff, D., Kao, T.-Y., Han, N., Chan, C. W. I., Cai, X., Yang, Y., Hayton, D. J., Gao, J.-R., Reno, J. L., and Hu, Q., "Terahertz laser frequency combs," *Nature Photonics* **8**(6), 462–467 (2014).

[10] Savchenkov, A. A., Ilchenko, V. S., Di Teodoro, F., Belden, P. M., Lotshaw, W. T., Matsko, A. B., and Maleki, L., "Generation of kerr combs centered at 4.5 μm in crystalline microresonators pumped with quantum-cascade lasers," *Optics letters* **40**(15), 3468–3471 (2015).

[11] Han, Z., Ren, D., and Burghoff, D., "Sensitivity of swift spectroscopy," *Optics express* **28**(5), 6002–6017 (2020).

[12] Burghoff, D., "Unraveling the origin of frequency modulated combs using active cavity mean-field theory," *Optica* **7**(12), 1781–1787 (2020).

[13] Benirschke, D. J., Han, N., and Burghoff, D., "Frequency comb ptychoscopy," *Nature Communications* **12**(1), 1–8 (2021).

[14] Pfeiffer, M. H., Liu, J., Raja, A. S., Morais, T., Ghadiani, B., and Kippenberg, T. J., "Ultra-smooth silicon nitride waveguides based on the damascene reflow process: fabrication and loss origins," *Optica* **5**(7), 884–892 (2018).

[15] Miller, S. A., Yu, M., Ji, X., Griffith, A. G., Cardenas, J., Gaeta, A. L., and Lipson, M., "Low-loss silicon platform for broadband mid-infrared photonics," *Optica* **4**(7), 707–712 (2017).

[16] Ramirez, J. M., Liu, Q., Vakarin, V., Le Roux, X., Frigerio, J., Ballabio, A., Alonso-Ramos, C., Simola, E. T., Vivien, L., Isella, G., et al., "Broadband integrated racetrack ring resonators for long-wave infrared photonics," *Optics letters* **44**(2), 407–410 (2019).

[17] Lee, Y.-J., Das, A., and Talghader, J. J., "High-q diamond microresonators in the long-wave infrared," *Optics express* **28**(4), 5448–5458 (2020).

[18] Kozak, D. A., Tyndall, N. F., Pruessner, M. W., Rabinovich, W. S., and Stievater, T. H., "Germanium-on-silicon waveguides for long-wave integrated photonics: ring resonance and thermo-optics," *Optics Express* **29**(10), 15443–15451 (2021).

[19] Hon, N. K., Soref, R., and Jalali, B., "The third-order nonlinear optical coefficients of si, ge, and si1- x ge x in the midwave and longwave infrared," *Journal of Applied Physics* **110**(1), 9 (2011).

[20] Liao, H.-Y., Jung, S., Chakravarty, S., Chen, R. T., and Belkin, M. A., "Low-loss ge-on-gaas platform for mid-infrared photonics," in [*2017 Conference on Lasers and Electro-Optics (CLEO)*], 1–2, IEEE (2017).

[21] Montesinos-Ballester, M., Vakarin, V., Liu, Q., Le Roux, X., Frigerio, J., Ballabio, A., Barzaghi, A., Alonso-Ramos, C., Vivien, L., Isella, G., et al., "Ge-rich graded sige waveguides and interferometers from 5 to 11 μm wavelength range," *Optics express* **28**(9), 12771–12779 (2020).

[22] Nedeljkovic, M., Penadés, J. S., Mitchell, C. J., Khokhar, A. Z., Stanković, S., Bucio, T. D., Littlejohns, C. G., Gardes, F. Y., and Mashanovich, G. Z., "Surface-grating-coupled low-loss ge-on-si rib waveguides and multimode interferometers," *IEEE Photonics Technology Letters* **27**(10), 1040–1043 (2015).

[23] Bai, Y., Bulsara, M. T., and Fitzgerald, E. A., "Photoluminescence and secondary ion mass spectrometry investigation of unintentional doping in epitaxial germanium thin films grown on iii-v compound by metal-organic chemical vapor deposition," *Journal of Applied Physics* **111**(1), 013502 (2012).

[24] Eaglesham, D. and Cerullo, M., "Low-temperature growth of Ge on Si (100)," *Applied physics letters* **58**(20), 2276–2278 (1991).

[25] Dziuban, J. A., "Bonding," *Bonding in Microsystem Technology* , 119–317 (2006).